Acta Cryst. (1969). A25, 82 C1·2

The Geometry of Integrated Intensity Measurement and Errors due to Non-Monochromatic Radiation

BY D. M. KHEIKER

Institute of Crystallography, USSR Academy of Science, Moscow, USSR

(READ BY S. C. ABRAHAMS)

Errors in the measurement of integrated intensity with a single-crystal diffractometer using non-monochromatic radiation are determined by: (i) the magnitude of the scan volume in reciprocal space, (ii) variation in truncation of the region around the reciprocal lattice points, (iii) incorrect determination of the background. The most accurate results are likely to be obtained by the use of suitable scanning procedure with the appropriate filters, combined with the correct estimation of aperture dimensions and their inclination.

1. The scan volume and scan methods

Errors and sensitivity

Increasing the scan volume in reciprocal space leads to an increase in background and a corresponding decrease in the precision and sensitivity of the measurements. This is evident in (1) and (2), where statistical error, ε_1, and the instability, ε_2, are defined:

$$\varepsilon_1 = \sqrt{(N+N_b)}/(N-N_b) \quad (1)$$

$$\varepsilon_2 = [(N\varepsilon)^2+(N_b\varepsilon)^2]^{1/2}/(N-N_b), \quad (2)$$

where N_b = the background count, N_d = the diffraction peak count, N = the total count, and ε = the relative magnitude of instability, when $N_b > N_d = N - N_b$, (1) and (2) reduce to (3) and (4) respectively.

$$\varepsilon_1 \approx \sqrt{2 \cdot \frac{1}{N_d} \cdot \frac{N_b}{N_d}} \quad (3)$$

$$\varepsilon_2 \approx \sqrt{2} \cdot \varepsilon \cdot \frac{N_b}{N_d} \quad (4)$$

For weak reflexions, statistical errors, ε_1, are proportional to the square root of the relative background, whereas non-stability errors ε_2, are directly proportional to the relative background.

Graphical model in the equatorial case

In Fig. 1 is depicted the reflecting circle, centre O_1, and a reciprocal lattice point whose dimensions (exaggerated) are a function of the actual experimental set-up. The dimensions are determined in practice by the following features:

$H\lambda$ – the length of the radius-vector in reciprocal space.
$\Delta\lambda$ – the spectral spread of the incident radiation.
M – the angular mosaic spread.
$x = (P+F)/R_r$ – the crossfire in the incident beam.

P and F are the dimensions of the specimen and source respectively while R_r is their separation. If the transverse dimension of the reciprocal lattice point is equal to $H\lambda(M+x)$ (Ladell, 1965), the diffracted beam is stationary. However it varies with x. The diffracted beam spreads over an angle x if segment x is oriented as in Fig. 1. This graphical model is only an approximate one, however, in that it does not take into consideration the spread of the diffracted beam source in the specimen volume.

The scan volume shape is determined by the width, b_c, and height, h_c, of the detector aperture, its axes of inclination τ, the scan interval, $\Delta\omega$, and the relation between the velocity of the crystal and that of the detector, *i.e.* ω or θ/θ or $\theta/2\theta$ scan.

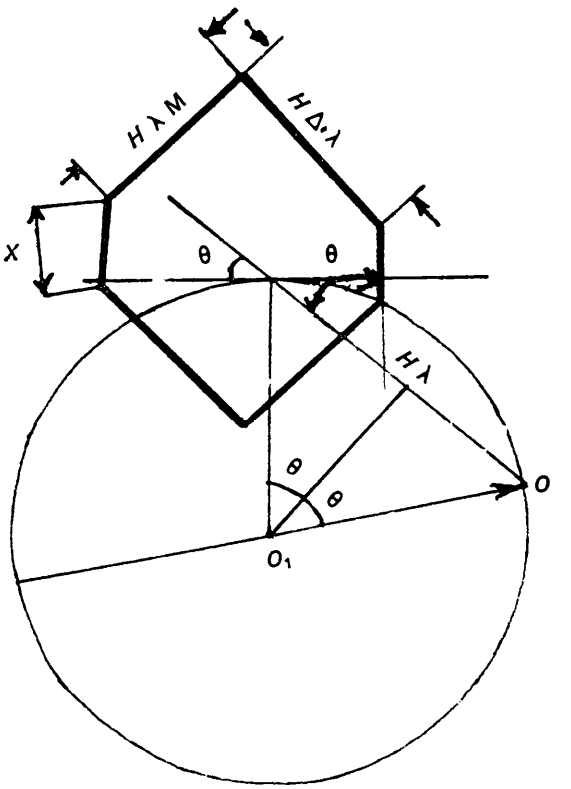

Fig. 1. Graphical representation of integrated intensity measurement in the equatorial case.

In order to minimize the scan volume, its shape must correspond as nearly as possible to that of the reciprocal lattice point, Fig. 1. To attain this end, the variables, b_c, h_c, τ and $\Delta\omega$ must be varied according to the scan method in use. The various possibilities are depicted in Fig. 2(*a*), (*b*) and (*c*) which correspond to the ω, θ/θ and $\theta/2\theta$ scans respectively. The equatorial section of the scan volume is shown shaded in each case, the base being the same in all three cases, namely

$$h_c = H\,\lambda\,M + x\,. \tag{5}$$

For Fig. 2(*a*), the detector is stationary and the scan volume is a parallelepiped with sides b_c^{ω}, h_c and the third edge is directed along the mosaic spread segment. For Fig. 2(*b*), which refers to the θ/θ scan, the sides of the scan volume are b_c^{θ} and h_c while the third edge is directed along the x segment. For Fig. 2(*c*), involving the $\theta/2\theta$ scan the corresponding dimensions are $b_c^{2\theta}$ and h_c, and the third edge of the parallelepiped is directed along the dispersive segment, $H\Delta\lambda$. The heights of all parallelepipeds are the same, being $H\,.\,\lambda\,.\,\Delta\omega\,.\cos\theta$. The best procedure to use to measure intensities is that for which the detector aperture width is smallest. Consideration of Fig. 2 suggests that preference should be given to the ω, θ/θ or $\theta/2\theta$ method depending on whether the M, x or $\Delta\lambda$ component predominates.

From Figs. 1 and 2, it is evident that the following relations hold.

$$b_c^{\omega}\cos\theta = H\,\Delta\lambda + x\cos\theta \tag{6}$$

$$b_c^{\theta}\,.\cos(2\theta - 90°) = H\,.\,\Delta\lambda\,.\sin\theta + H\,\lambda\,M\cos\theta \tag{7}$$

$$b_c^{2\theta}\,.\sin\theta = H\,\lambda\,M + x\,.\sin\theta \tag{8}$$

$$H\,.\,\lambda\,.\,\Delta\omega = b_c^{2\theta}\,.\sin\theta + b_c^{\omega}\,.\sin\theta \tag{9}$$

and from (5)–(9), the following relations:

$$b_c^{\omega} = 2\cdot\frac{\Delta\lambda}{\lambda}\cdot\tan\theta + x + P/R_r \tag{10}$$

$$b_c^{\theta} = \frac{\Delta\lambda}{\lambda}\cdot\tan\theta + M + P/R_r \tag{11}$$

$$b_c^{2\theta} = 2M + x + P/R_r \tag{12}$$

$$h_c = 2M\sin\theta + x + P/R_r \tag{13}$$

$$\Delta\omega = \frac{\Delta\lambda}{\lambda}\cdot\tan\theta + M + x\,. \tag{14}$$

The term P/R_r in (10)–(13) is a measure of the maximum separation of beams diffracted from the specimen. The correspondence of the values derived for h_c and the various b_c with those of Alexander & Smith (1962, 1964*a*, 1964*b*), Burbank (1964) and of Ladell & Spielberg (1963) is not exact because the graphical model is an approximate one. Thus, for example, the trigonometric terms associated with the P/R_r terms do not appear.*

Graphical model in the equi-inclination case

For the equi-inclination setting, Burbank (1964) obtained the following result: the diffracted beams for one reflexion and different wavelengths λ are approximately in the same plane, which is inclined towards the equatorial plane at a constant angle for a given reflexion angle, τ. Consequently, in the equi-inclination diffractometer, using an ω-scan, one can use a detector aperture calculated for the equatorial setting with its axes inclined at an angle τ or calculate dimensions of the aperture for the usual setting. Kheiker, Gorbaty

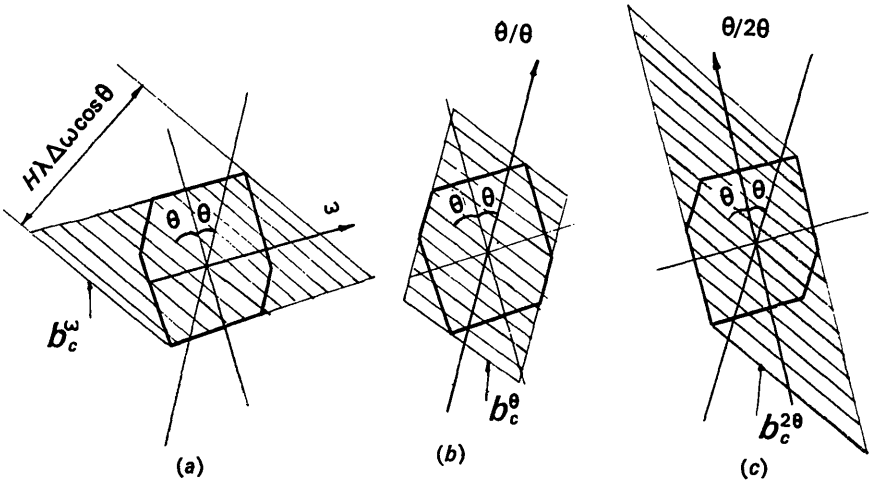

Fig. 2. Scanning volumes for different scanning methods. Equatorial setting.

& Lube (1968) obtained relationships for the general case of inclination setting between the scan range, $\Delta\omega$, the aperture width, b_c, and height, h_c, for the ω and $\omega/2\omega$ scan. In the latter case, the following graphical model was used: the family of reflexion spheres which are connected with primary beams with crossfire, $x=(P+F)/R_r$, have reciprocal lattice points with dimensions $H\Delta\lambda$ parallel and $H\,\lambda\,M$ perpendicular to

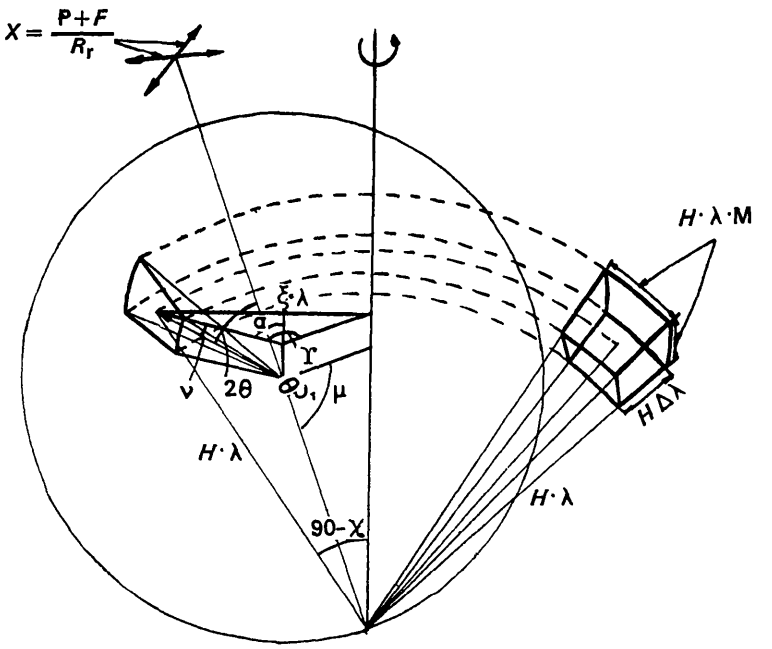

Fig. 3. Graphical representation of integrated intensity measurement in the case of general inclination geometry.

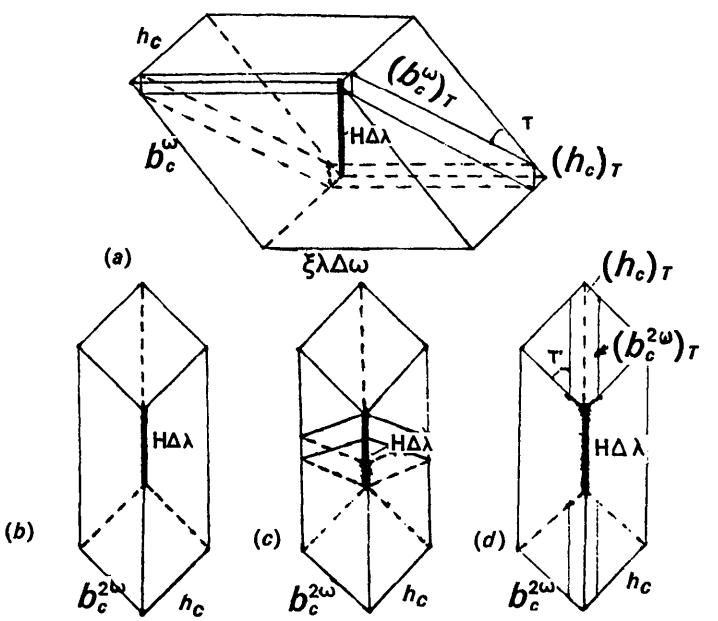

Fig. 4. Scanning volumes for dispersive strip: (*a*) ω-scan with normally oriented aperture axes, and with axes inclined through angle $\tau=\text{arctg}\,h_c/b_c{}^{\omega}$. (*b*) $\omega/2\omega$-scan, normally oriented aperture axes. (*c*) $\omega/2\omega$-scan with a second stationary slit with axes inclined through an angle τ. (*d*) $\omega/2\omega$-scan with moving slit inclined through angle $\tau=\text{arctg}\,h_c/b_c{}^{2\omega}$.

the radius $H\lambda$, Fig. 3. The same approximation was used as in the case of the equatorial setting in respect of the displacement of diffracted beam sources.

$$\Delta\omega = \frac{\Delta\lambda}{\lambda}\left|\left(\tan\alpha + \frac{\tan\chi\tan\nu}{\cos\alpha}\right)\right| + M\left|\left(\tan\chi\tan\alpha - \frac{\tan\nu}{\cos\alpha}\right)\right| + M\cdot\left|\frac{1}{\cos\chi}\right| + x\left(\left|\frac{1}{\cos\mu}\right| + \left|\frac{\cos\mu\,.\tan\nu - \sin\mu\,.\cos\Upsilon}{\xi\lambda\cos\alpha}\right|\right) \quad (15)$$

* *Note added in proof*: – The model just considered can be refined in the following way. Let us consider in the equatorial cross-section of the specimen, the direction lying in the focusing plane and perpendicular to the latter. Rotating the spherical specimen through an angle $P\sin\theta/R_r$ will lead to displacement of the reflexion zone along the focusing plane, the ends of the diffracted rays being directed a as result of focusing on one point. Consequently, to the mosaic angle should be added an angle $P\sin\theta/R_r$. Upon displacement of the reflexion zone along the normal to the focusing plane the specimen should be rotated through an angle $P\cos\theta/R_r$ while the counter should be rotated through an angle $2P\cos\theta/R_r$, *i. e.* the term $P\cos\theta/R_r$ is to be added to the dispersion term $\Delta\omega_\lambda = (\Delta\lambda/\lambda)\,\mathrm{tg}\,\theta$. It thus follows that the dimensions given below should be substituted for those shown in Figs. 1 and 2.

$$x \to P/R_r$$

$$H\Delta\lambda \to H\Delta\lambda + 2\frac{P}{R_r}\cos^2\theta$$

$$H\lambda M \to H\lambda\left(M + \frac{P}{R_r}\sin\theta\right).$$

It this case we obtain formulae which differ in no way from those presented by the authors cited above.

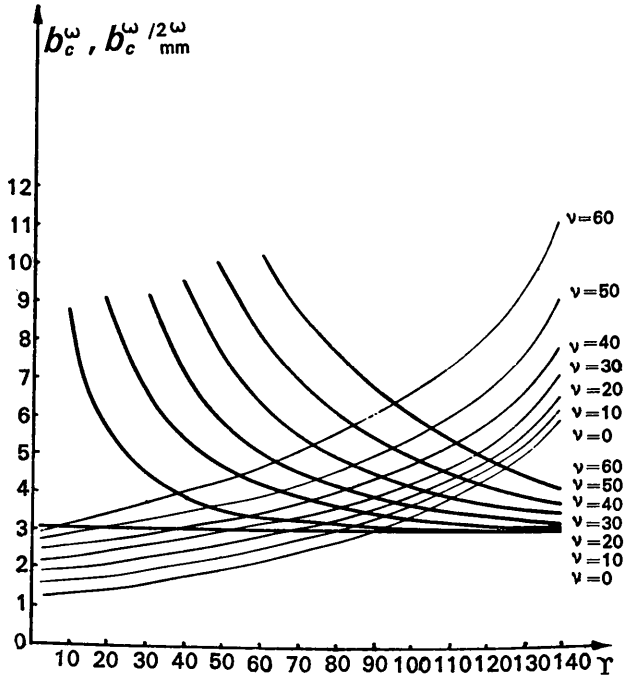

Fig. 5. Counter slit width for ω-scan and $\omega/2\omega$-scan in equi-inclination setting. Slit axes are directed as usual. b_c^ω fine line, $b_c^{\omega/2\omega}$ fat line.

$$b_c^\omega = \sum_i |\cos\nu\,.\,\Delta\Upsilon_i| + |P/R_r| = \frac{\Delta\lambda}{\lambda}\left|\left\{\frac{\xi\,.\,\lambda}{\cos\alpha} + (\sin\nu - \sin\mu)\tan\nu\,.\tan\alpha\right\}\right| + M\left|\left(\frac{\sin\nu - \sin\mu}{\cos\alpha} - \xi\,.\,\lambda\,.\tan\nu\,.\tan\alpha\right)\right| + x\left\{\left|\frac{\cos\nu}{\cos\mu}\right| + \left|\cos\mu\tan\nu\tan\alpha - \sin\mu(\cos\Upsilon\,.\tan\alpha - \sin\Upsilon)\right|\right\} + |P/R_r| \quad (16)$$

$$b_c^{2\omega} = \cos\nu\sum_i |2\Delta\omega_i - \Delta\Upsilon_i| + \left|\frac{P}{R_r}\right| \quad (17)$$

$$h_c = \frac{\Delta\lambda}{\lambda}\cdot\left|\frac{\sin\nu - \sin\mu}{\cos\nu}\right| + M\cdot\left|\frac{\xi\,.\,\lambda}{\cos\nu}\right| + x\cdot\left|\frac{\cos\mu}{\cos\nu}\right| + \left|\frac{P}{R_r}\right|. \quad (18)$$

The various symbols are indicated in Fig. 3.

From equations (15) to (18), one can obtain the respective relationships for the equi-inclination setting by substituting $\mu = -\nu$, for the flat-cone setting by placing $\nu = 0$ and for the normal-beam setting with $\mu = 0$. Dispersive and mosaic spread terms can be derived if the scan volume and the reciprocal lattice point volume is considered by analogy with the equatorial setting. This enables a decision to be reached as to which technique is to be preferred for the measurement of integrated intensity. For the equi-inclination setting, a scan volume and a reciprocal lattice point whose dimensions are determined by a dispersive component only, are depicted in Fig. 4. Fig. 4(*a*) shows the scan volumes for ω-scan with aperture axes oriented normally and with those inclined through angle $\tau = \arctan h_c/b_c^\omega$. The scan volume for an $\omega/2\omega$-scan with axes normally oriented is shown in Fig. 4(*b*) while Fig. 4(*c*) shows the scan volume with a second stationary slit, this slit's axes being inclined through an angle τ. The situation for $\omega/2\omega$ scan with a moving slit which is inclined at an angle $\tau' = \arctan h_c/b_c^{2\omega}$ is shown in Fig. 4(*d*). Fig. 5 shows b_c^ω and $b_c^{2\omega}$ functions for equi-inclination settings corresponding to (16) and (17) for $\mu = -\nu$, $\Delta\lambda/\lambda = 0{\cdot}007$, $M = 0{\cdot}006$, $x = 0{\cdot}006$ and $P/R_r = 0{\cdot}003$. Consideration of these curves suggests the following conclusions: ω scan should be used at low Υ-angles and $\omega/2\omega$ scan at high Υ-angles. Use of the two scan techniques would lead to an effective reduction of detector aperture compared with the use of one or other over the whole range of Υ. This result is also correct for other inclination settings. The method of combination is used in preference at high υ-angles and low ν-angles, as compared

with ω-scan with inclined aperture axes. The devising of a mechanical device on the diffractometer to permit use of the combined method is relatively straightforward. To apply it effectively, the computer must compare the aperture dimensions for different scanning techniques and select that which corresponds to the smallest aperture (Lube & Kheiker, 1968). Combining $\omega/2\omega$ scan with the moving inclined counter slit, Fig. 4(*d*), leads to a further reduction of scan volume.

2. Variation of truncation of a reciprocal lattice point

The spectral distribution of the incident beam is approximated by a Cauchy function whereas the mosaic orientation distribution is represented by a Gaussian function. The effective limits of the reciprocal lattice point correspond to the specified level of the given function and will remain essentially constant for each reciprocal lattice point. The scan volume may therefore contain only part of the reciprocal lattice point. Due to the approximations involved in the model and the errors in the calculation introduced by use of a summation procedure rather than a convolution, the component of the reciprocal lattice point actually recorded will change from one reflexion to another. The specific error introduced by this change of the scan volume relative to the reciprocal lattice points is called the 'truncation' error. For the equatorial setting, the scan component was obtained as a function of θ-angle by Alexander & Smith (1962) using convolution procedures. The comparison of the results from summation procedures with those from convolution allows values for the truncation error to be derived. For $\Delta\lambda = \Delta\lambda_{K\alpha1-K\alpha2} + 4(\Delta\lambda_{K\alpha1} + \Delta\lambda_{K\alpha2})$ where $\Delta\lambda_{K\alpha1-K\alpha2}$ is the separation of the $\alpha_1\alpha_2$ components and $\Delta\lambda_{K\alpha1}$, $\Delta\lambda_{K\alpha2}$ are the half-widths of $\alpha_1\alpha_2$, the scan component changes from 96% to 93% for $2\theta \sim 100°$ to 160°. For $\Delta\lambda = \Delta\lambda_{K\alpha1-K\alpha2} + 10(\Delta\lambda_{K\alpha1} + \Delta\lambda_{K\alpha2})$, the corresponding change is 98·5% to 97%. To decrease error from this source, the scan volume must be increased. The advisable scan range is determined by the given level of the 'truncation' error, a compromise between the requirements of this section and those in section 1 being necessary for optimum results.

3. Determination of the background

The diffraction peak is superimposed on a background. Using non-monochromatic radiation in the primary beam, estimation of the background may have to be

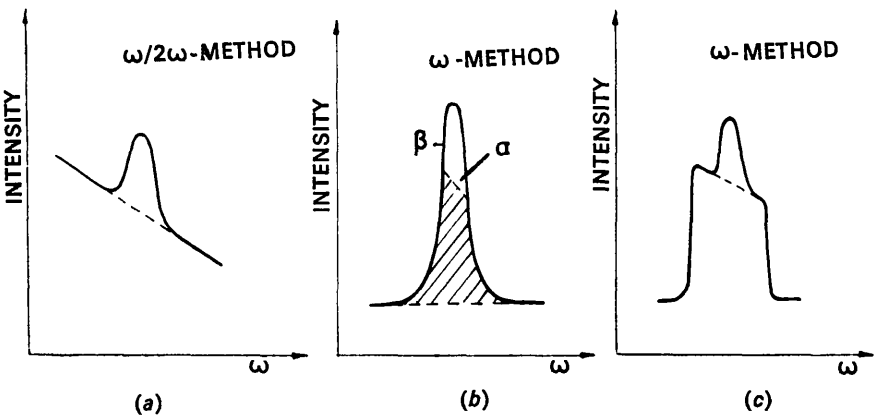

Fig. 6. Error due to incorrectly selected aperture. Background strip is along $H\lambda$.

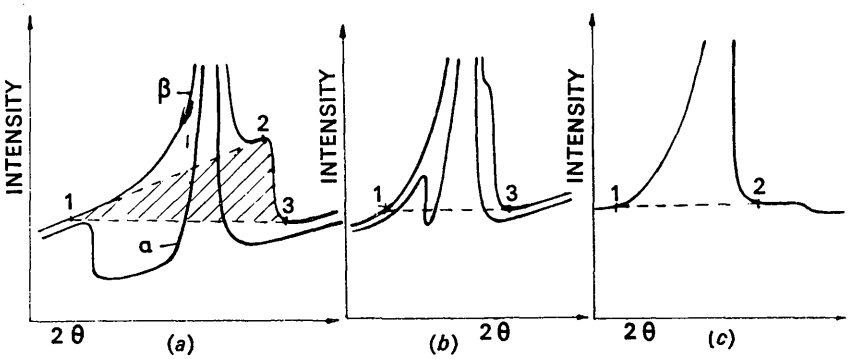

Fig. 7. Error due to non-monotonic background; Bragg reflexion with non-monochromatic spectrum, (*a*) medium angles, (*b*) low angles, (*c*) high angles.

made on the basis of an approximately linear dependence of the background intensity on the angle ω.

The basic components contributing to the background distribution are as follows:

(1) Bragg reflexion of non-characteristic radiation.
(2) Fluorescent and Compton radiation.
(3) Scatter from air and any other obstacles.
(4) Thermal diffuse scattering.
(5) Background of the quantum counter.

The first component is non-monotonic along the radius vector in reciprocal space due to such features as absorption edges, and the shape of the non-characteristic spectral distribution, *etc.* and is non-linear in the transverse direction due to the mosaic spread and the distribution of x. The third component is non-linear at low and high angles along the radius vector in reciprocal space; see Young (1965), Fig. 8. These errors may be diminished experimentally by decreasing the primary beam cross-section, extending the specimen mounting fibre and by using a good beam trap. The thermal diffuse scattering is markedly non-linear, see Cochran (1969) {Paper in these proceedings}. The other components weakly depend on ω. The first background component is located along the radius vector in reciprocal space, and the width of the counter slit for an ω-scan must be $b_c^{\omega}+2b_c^{2\theta}$ as is evident from Fig. 2(*a*) and (*c*). If the aperture dimensions have been selected correctly, the profiles of the diffraction peak are identical for all the scan methods, Fig. 6(*a*) and (*c*). The profiles derived by the different procedures may, in such circumstances, be distinguished by the level of the background. If the detector aperture dimensions are smaller than those correctly calculated, then the profiles are different. If balanced filters are used, the slit width should be b_c^{ω} as follows from section 1 of the present paper [Fig. 6(*b*)].

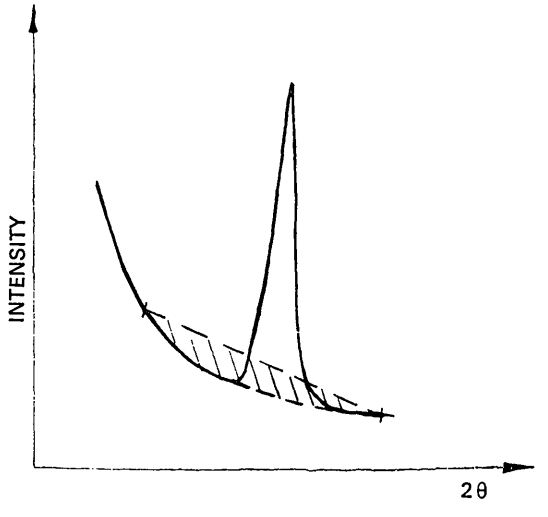

Fig. 8. Error due to non-linear background, caused by parasitic and air scattering.

Bragg reflexion from non-monochromatic radiation leads to a non-monotonic distribution along the radius vector only at low angles. In this region, the dispersion is small and $\Delta H/H$ is large (ΔH corresponds to the distance between neighbouring reciprocal lattice points). At high angles, dispersion is considerable but $\Delta H/H$ is smaller, the spectra are superimposed and therefore, in this region, the background component becomes smooth.

The non-monotonic background near the absorption edge of a β-filter leads to incorrect measurement of the background, Fig. 7. At very low angles, the background will be measured as 1–3 in Fig. 7(*b*), while at medium and high angles it will be as 1–2 in Fig. 7(*a*) and (*c*). To minimize error, measurements at low angles should be carried out with balanced filters and in this case the following appropriate conditions must apply, $\Delta\lambda/\lambda < 1/h$. The relative width of a balanced filter band pass is $\Delta\lambda/\lambda \sim 2/Z$ where Z is the atomic number of the anode material. For Cu $K\alpha$ radiation, $\Delta\lambda/\lambda \sim 0{\cdot}07$, for Mo $K\alpha$ 0·05. Hence, with balanced filters, 14 and 20 orders respectively can be measured. This corresponds to a limit of $2\sin\theta = h\lambda/a$. For $a = 20$ Å and Cu $K\alpha$ radiation, $2\sin\theta = 1{\cdot}08$, for Mo $K\alpha$, 0·70. Measurements with balanced filters can be carried out in the central part of the reciprocal lattice in accord with the conditions mentioned. The transition from β to $\alpha-\beta$ (balanced filters) measurements has to be determined experimentally.

The most accurate results may be obtained by a combination of different scanning and different filter techniques with detector aperture dimensions correctly calculated and appropriately inclined.

References

ALEXANDER, L. E. & SMITH, G. S. (1962). *Acta Cryst.* **15**, 983.
ALEXANDER, L. E. & SMITH, G. S. (1964*a*). *Acta Cryst.* **17**, 447.
ALEXANDER, L. E. & SMITH, G. S. (1964*b*). *Acta Cryst.* **17**, 1195.
BURBANK, R. D. (1964). *Acta Cryst.* **17**, 434.
COCHRAN, W. (1969). *Acta Cryst.* A**25**, 95.
KHEIKER, D. M., GORBATY, L. W. & LUBE, E. L. (1968). *Soviet Phys. Cryst.* In the press.
LADELL, J. (1965). *Trans. Amer. Cryst. Ass.* **1**, 86.
LADELL, J. & SPIELBERG, N. (1963). *Acta Cryst.* **16**, 1057.
LUBE, E. L. & KHEIKER, D. M. (1968). *Apparatus and Methods in* X-*ray Diffraction Analysis*, No. 3. (U.S.S.R.) p. 145.
YOUNG, R. A. (1965). *Trans. Amer. Cryst. Ass.* **1**, 42.

DISCUSSION

COCHRAN: Does the truncation error arise because not all the white radiation is included or because even the $K\alpha_1\alpha_2$ component is not included? If the latter, I cannot see why one should accept any truncation error at all.

ABRAHAMS: The truncation error appears to be due to the fact that summation is not over the full volume of reciprocal space which ought to be covered.

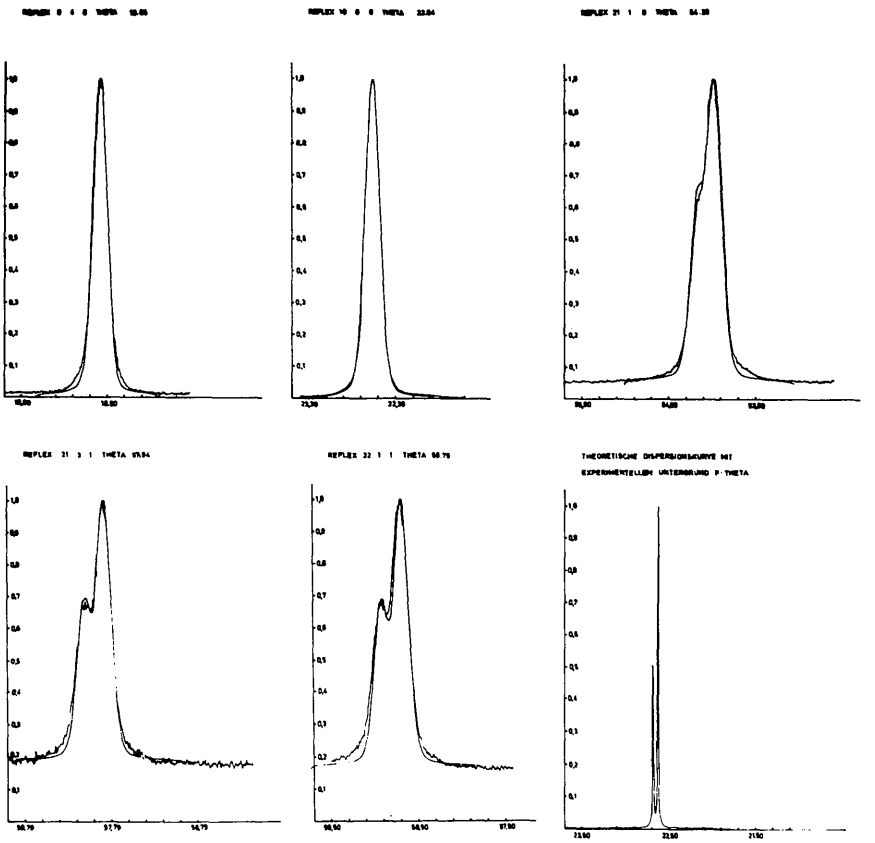

Fig. 9. Profiles of various reflexions calculated and plotted by computer compared with the experimental profiles.

SHOEMAKER: It is our interpretation that it is meant only to include $\alpha_1\alpha_2$.

COCHRAN: In that case, a truncation error of 7% (say) seems excessive.

ALEXANDER: A truncation error arises from the uncertainty of the shape of the characteristic radiation spectral line.

FURNAS: A paper on a closely similar topic, the appropriate size of apertures, by R. Einstein of Oak Ridge, should appear in print in the near future.

ABRAHAMS: One can get profiles and integrate them but the result does not necessarily yield integrated intensity values. This appears to be the conclusion of Dr Kheiker's paper.

HOPPE: It may be of interest to refer here to an alternative procedure in treating background which Dr G. Kopfmann and I have developed.

In principle, there is a very simple way to cope with background problems. A tube delivers a mixture of white radiation and of characteristic radiation. If the spectrum – as seen from the counter – is known (that means that it has been measured), and if all structure factors are known, the whole intensity distribution produced by this source of polychromatic radiation can be calculated. If the structure factors have been determined in the conventional way, their convolution will produce not only the crystal reflexions again but also the background, due to the white radiation. This leads to a better background correction and, therefore, also to better structure factors. This process can be repeated. We call this procedure 'computational monochromatization'. This computation of the influence of the white radiation can be done quite accurately. It is especially important that it will show regions where the background has abnormal shape, *e.g.* in the neighbourhood of strong reflexions, or is caused by unwanted characteristic wave lengths in the spectrum.

In practice, these computations are quite complicated as all factors which influence the profile of a reflexion (divergence, mosaicity, crystal size, absorption) have to be taken into account. Fig. 9 shows calculated profiles of different reflexions against their experimental profiles. There is good overall agreement. The small deviations near the reflexions may be due to thermal diffuse scattering. The last figure in the second row shows the spectrum of the tube. It should be mentioned that the profile of the characteristic radiation was calculated (from the experimental values), as the resolution of our instrument was too low.

In the ideal case this scheme should permit intensity measurements without background measurements. In practice, however, some measurements have to be made in order to scale for factors which have not been properly corrected in the computations (*e.g.* Compton scattering, multiphonon thermal scattering, fluorescence radiation).